Orientation of Platelets in Multilayered Nanocomposite Polymer Films*

MATTHEW M. MALWITZ,[1] SHENG LIN-GIBSON,[2] ERIK K. HOBBIE,[2] PAUL D. BUTLER,[3] GUDRUN SCHMIDT[1]

[1]Louisiana State University, Baton Rouge, Louisiana 70803

[2]Polymers Division, National Institute of Standards and Technology, Gaithersburg, Maryland 20899

[3]Oak Ridge National Laboratory, Oak Ridge, Tennessee 37831

Received 30 January 2003; revised 12 May 2003; accepted 16 June 2003

ABSTRACT: The orientation of platelets in micro-meter-thick polymer–clay nanocomposite films was investigated with small-angle neutron scattering (SANS), small-angle X-ray scattering (SAXS), and wide-angle X-ray diffraction (WAXD). The films with various clay contents (15–60% by mass fraction) were prepared by a layer-by-layer approach from polymer–clay solutions that led to the formation of a high degree of orientation in both polymer and clay platelets. Shear-induced orientation of polymer–clay solutions is compared with the orientation of polymer–clay films. SANS, SAXS, and WAXD, with beam configurations in and perpendicular to the spread direction of the film, were used to determine the structure and orientation of platelets. In all films, the clay platelets oriented preferentially in the plane of the film. The observed differences in semidilute solutions, with clay surface normal parallel to the vorticity direction, versus bulk films and with clay surface normal parallel to the shear gradient direction at clay mass fractions of 40 and 60%, were attributed to the collapses of clay platelet during the drying process. © 2003 Wiley Periodicals, Inc. J Polym Sci Part B: Polym Phys 41: 3237–3248, 2003

Keywords: poly(ethylene oxide); clay; nanocomposites; orientation; scattering

INTRODUCTION

Ordering platelets at the nanometer length scale is a challenging and active research area in materials science.[1–4] Unique or enhanced mechanical,[1,5] electrical,[6] optical,[6,7] and thermal properties[1,8–14] have been observed in solution and in bulk clay containing nanocomposites. Such enhancements arise from the physical presence of nanoparticle, the interactions between the polymer and particle, and the state of dispersion.[1,15–17] Approaches developed to date range from manipulation of individual particles to exploitation of self-assembly in colloids.[18] The large aspect ratio of the platelets also promotes the formation of supramolecular organizations similar to other mesoscopic systems, such as liquid-crystalline polymers,[19–22] surfactants,[23] and block copolymers.[24,25] Multicomponent systems may generate new structures with hybrid properties. In this article, we focus on the preparation and structural characterization of polymer–clay films prepared by a layer-by-layer approach from polymer–clay solutions. Efficient nanoparticle dispersion in solution combined with good poly-

Certain equipment and instruments or materials are identified in this article to adequately specify the experimental details. Such identification does not imply recommendation by the National Institute of Standards and Technology nor does it imply the materials are the best available for the purpose.

Correspondence to: G. Schmidt (E-mail: gudrun@lsu.edu)

Journal of Polymer Science: Part B: Polymer Physics, Vol. 41, 3237–3248 (2003)

mer–particle interfacial adhesion allows the exciting possibility of developing strong and transparent films,[1,26,27] coatings, and membranes. Hybrid films such as the ones described in this article may offer exciting opportunities for a wider range of applications.

The effect of shear on the orientation of polymer–clay nanocomposites has been examined by a number of groups,[4,28–30] and in some cases, the three-dimensional (3D) orientation of the polymer and clay has been determined.[31–33] The two-dimensional (2D) clay may align in three primary directions under shear, often referred to as a, b, and c orientations.[23] In the perpendicular, or a orientation, the surface normal aligns parallel to the vorticity direction, and the particles lie in the flow-gradient plane; in the transverse, or b orientation, the surface normal aligns parallel to the flow direction, and the particles lie in the vorticity-gradient plane; in the parallel, or c direction, the surface normal aligns parallel to the shear gradient direction, and the particles lie in the flow-vorticity plane.

The general or intuitive response of the clay platelet orientation in a polymer matrix is in the c orientation. This has been described by studies such as for nylon–clay nanocomposites.[1,4] Studies with *in situ* X-ray diffraction provide direct evidence for rheology-microstructure linkages in polypropylene nanocomposites.[34] Recent transmission electron microscopy (TEM) analysis has revealed a house-of-cards structure in polypropylene–clay nanocomposite melts under elongational flow.[35] Strong strain-induced hardening and rheopexy features at higher deformation originated from the perpendicular alignment of the silicate to the stretching direction (b orientation). Although TEM is not an *in situ* technique, it did reveal the differences in the shear flow-induced versus elongational internal structures of the nanocomposite melt. These nanocomposites have strong interactions between the polymer matrix and the silicate layers.

Small-angle X-ray scattering (SAXS) is a powerful technique commonly used to characterize the nanocomposite structure and provide a measure of nanoparticle orientation.[19,20,22,32] Scattering from an anisotropic distribution of particles results in an anisotropic scattering pattern. Measuring the scattering patterns in two dimensions with a Couette flow cell in the radial and tangential configurations allow for the unambiguous determination of the orientations of polymer and clay in solutions under shear.[36–38] An unexpected case of 'a' orientation was observed for aqueous solutions of synthetic Laponite clay and poly(ethylene oxide). The polymer and clay interact in a dynamic adsorption–desorption equilibrium to form a network.[38] Small-angle neutron scattering (SANS) on samples in D_2O measured the shear-induced orientation of polymer and platelets. SANS on contrast-matched samples detected the orientation of the polymer alone. With increasing shear rate, the clay particles orient first, and then the polymer chains start to stretch.[36] As the shear distorts and ruptures the transient gel, coupling between composition and shear stress leads to the formation of spatially modulated macrodomains.[39] We have proposed[39] that the clay orients in response to a biaxial stress arising from shear and elastic forces.

The objective of this contribution was to prepare polymer nanocomposite multilayered films with a defined orientation with networklike solutions as previously described by us[36] and to determine if and how the shear orientation in the solution can be maintained when the solvent is evaporated. The multilayered structures that we have developed and examined may be important for many applications, such as microelectronics, optical devices, or chemical sensors.[40] Scattering and diffraction measurements are used to investigate the shear-induced orientation of polymer and platelets in nanocomposite films. First, we examine films derived from well-dispersed synthetic laponite clay and then compare the results with those derived from the montmorillonite dispersions.

EXPERIMENTAL

Synthetic and natural clay, laponite and montmorillonite, respectively, were used in this study. The clay platelets were comprised of three layers with a center magnesium ion layer sandwiched between two silicate layers. The synthetic hectorite-type clay, laponite RD (LRD), provided by Southern Clay Products,[41,42] consists of clay platelets of high purity and uniform crystallite size.[12,13] The natural smectite montmorillonite clay is Cloisite NA+ (CNA). The platelet diameter (the platelet dimension in the plane of the platelet) is on the order of 300 Å for laponite and between 700 and 1500 Å for montmorillonite, with a thickness of approximately 10 Å. The smaller laponite diameter results in a smaller aspect ratio (30:1) than for montmorillonite (100:

Table 1. PEO/Clay Film Characteristics

Sample	Mass Fraction, % Clay
LRD15	15
LRD40	37
LRD60	60
CNA40	33

Relative mass error: <1%.

1). Under appropriate conditions, laponite and montmorillonite platelets may completely exfoliate in aqueous solutions.[43,44] Poly(ethylene oxide) (PEO) [weight-average molecular weight (M_w): 10^6 g/mol, molecular mass distribution: ca. 1.5] was purchased from Polysciences, Inc. All reagents were used as received.

PEO-clay films were prepared from exfoliated polymer–clay solutions via a layer-by-layer spreading approach. PEO and various concentrations of LRD were prepared in distilled, deionized water and mixed for at least 4 weeks until optimally exfoliated and transparent dispersions are obtained.[38] The solution pH and ionic strength were controlled by the addition of NaOH and NaCl, respectively. A pH value of 10 and a NaCl concentration of 10^{-3} mol/L were used for all samples. Under these conditions, flocculation due to the dominance of van der Waals attraction over electrostatic repulsion of the clay as well as degradation of the clay particles is avoided. Solutions were spread on glass slides, layer by layer, and dried at 25 °C in desiccators and *in vacuo*. More detailed film preparation is described in the literature.[45] During the drying process, there is no sedimentation of clay particles. Transparent single films with an average layer thickness of 5–7 μm were obtained by manually spreading the polymer–clay gel on a glass substrate with a blade.

For comparison, nonoriented bulk samples prepared by simply drying PEO-LRD solutions without spreading and therefore without any mechanical orientation are also investigated. Although the bulk samples have the same characteristics as those prepared by the layer-by-layer approach, they are significantly thicker (between 2 and 3 mm) than the multilayer films (between 5 and 7 μm, see Table 1).

SANS measurements were performed on the 30-m SANS NG7 instrument at the Center for Neutron Research, National Institute of Standards and Technology (NIST).[46] In a standard *y*-beam configuration, the incident beam is perpendicular to the spread direction of the film and the SANS intensity is obtained in the *x*-*z* plane. In the *z*-beam configuration, the incident beam is parallel to the spread direction of many stacked PEO-clay films (see Figs. 1 and 2). The neutron beam in the z-beam configuration provided SANS intensities in the *x*-*y* plane. Sample-to-detector distances of 15 and 4 m and incident wavelengths (λ's) of 8.44 and 5 Å were used to give q ranges ($q = 4\pi/\lambda \sin(\theta/2)$ of 0.0008221 $Å^{-1} < q < 0.01515$ $Å^{-1}$ and 0.00898 $Å^{-1} < q < 0.08621$ $Å^{-1}$). Because of the longer wavelength, neutron scattering probes structure at longer length scales than typical X-ray scattering. The primary contrast in the SANS experiment is between the silicate and PEO. This allows SANS experiments to detect the overall orientation of the clay platelets in polymer matrix.

Time-resolved SAXS and wide-angle X-ray diffraction (WAXD) measurements were performed at the Advanced Polymers Beamline (X27C) at the National Synchrotron Light Source (NSLS), Brookhaven National Laboratory (BNL). The wavelength of the X-ray beam was 1.366 Å. The beam size was 0.4 mm in diameter at the sample position. Synchrotron X-rays were collimated with a three 2° tapered tantalum pinhole collimator. The sample-to-detector distance used was 1.73 m for SAXS. The SAXS scattering angle was calibrated with silver behenate, and the intensity was normalized by incident beam fluctuations. The relative uncertainty associated with the X-ray measurement was ±5%.

There is a possibility that voids and porosity may influence the total scattering intensity. Thermogravimetric analysis on representative films and differential scanning calorimetry (DSC) detected the presence of about 0.5% water in our films.[47] Research by other groups[40] has demonstrated that composite films prepared by alternate adsorption of polymer and exfoliated sheets of a synthetic laponite may respond in a dramatic way to changes in ambient humidity. Residue water molecules in our films should be distributed homogeneously and do not affect the structure and orientation of clay platelets in the film.

RESULTS AND DISCUSSION

Polymer–clay solutions were used to prepare nanocomposite films with well-defined clay platelet orientations through a layer-by-layer ap-

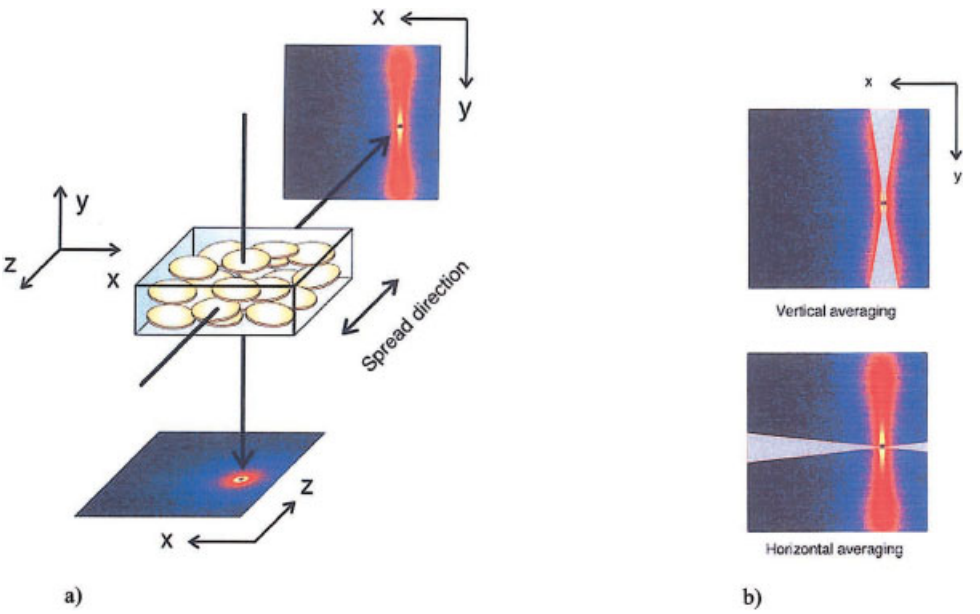

Figure 1. (a) With the clay platelets aligned in the spread direction of the film (*x*-*z* plane), we observe an anisotropic SANS pattern with the neutron beam in *z* configuration and an isotropic SANS pattern with the beam oriented in *y* configuration. (b) SANS intensity is averaged from 10° sectors in the horizontal (*x*) and vertical directions (*y* or *z*) of the 2D SANS patterns. This procedure allowed us to obtain SANS intensities for each of the three directions in space.

proach. The orientation of polymer and/or clay platelet will greatly affect various properties, such as mechanical and barrier properties, of the nanocomposite films. Our previous work focused on determining the polymer–clay solution orientation; in this study, we determine the orientation of the polymer–clay films that have been prepared with polymer–clay solutions.

There has been new technology of adsorption from solution for the fabrication of molecularly ordered multicomposite films to expand and replace the well-known Langmuir–Blodgett techniques and to open the field of molecular self-assembly to materials science.[48,49,50] For example, an atomic force microscopy (AFM) study on multilayered clay films revealed that polymer-laponite films are characterized by significantly higher surface coverage than natural clays.[48] Similar to systems that have been investigated,[51] the films used in our work were prepared by sequential adsorption of a polymer–clay gel. The preparative method used by us offers a powerful strategy to building ordered films by shear orientation from solution. One major motivation to use the spreading and drying procedure for PEO-clay nanocomposites containing 40–60% clay by mass fraction is the ability for preparing well-dispersed and oriented nanocomposites, which would otherwise be nearly impossible to prepare with conventional bulk mixing. Spin-casting of polymer–clay solutions was also problematic because of high-solution viscosity and elasticity as well as difficulties in removing the impurities.

The surface morphology and roughness of similar but one-layer films (5 μm thick) has been characterized by AFM.[1] Although strong concentration dependence was observed on film morphology, no anisotropy could be detected. Because our nanocomposite films were prepared by spreading a thin layer of polymer–clay solution followed by drying and then repeating this process in the same spread direction several times until a multilayer film of approximately 1 mm thickness was obtained, it was important to examine whether an interface exists between each layer. Our preliminary scanning electron microscopy (SEM) studies could not detect boundaries between single-spread micro-meter-thick film layers but surprisingly showed a highly ordered and layered structure in the *x*-*y* plane and fractal-like structures in the *x*-*z* plane.[47] Additional SEM studies also suggested that the exact thickness of

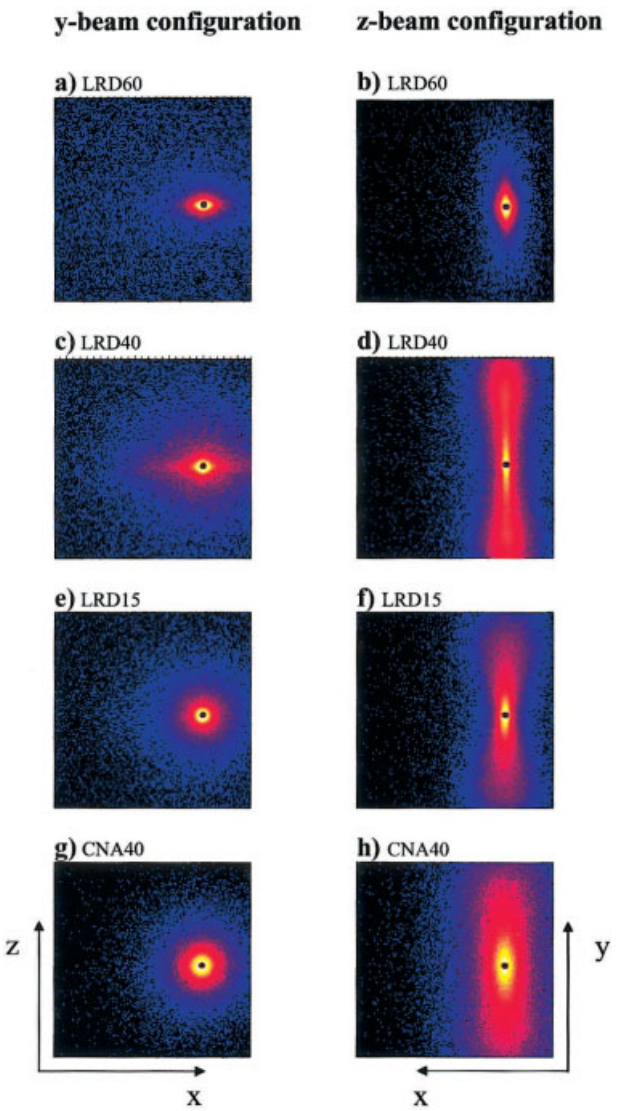

Figure 2. 2D SANS patterns from samples described in Table 1. The neutron beam in *z* configuration gives SANS patterns in the *x*-*y* plane, and with the beam oriented in *y* configuration we obtain SANS intensity in the *x*-*z* plane. [Color figure can be viewed in the online issue, which is available at www.interscience.wiley.com]

one dried layer is not important to the overall orientation of platelets.

Various scattering and diffraction techniques can be used to analyze the clay orientation. Figure 1 depicts 2D SANS patterns obtained in the *y*- and *z*-beam configurations for LRD40. The orientation of the clay platelet can be deduced from these results, and the physical picture is illustrated in the schematic [Fig. 1(a)] in which the predominant orientation of the clay platelets is the c orientation with a surface normal perpendicular to the film plane. As shown in detail, the orientation of clay observed in solution, the a orientation, was preserved only to a small degree in some compositions when the solvent was evaporated.

SANS results obtained for PEO-LRD nanocomposite films with various clay contents and a PEO-CNA nanocomposite film in the *y*- and *z*-beam configurations are shown in Figure 2. 2D scattering patterns obtained in the *y*-beam configuration show slight anisotropy for LRD60 and LRD40 but not for LRD15 and CNA40. Scattering patterns obtained in the *z*-beam configuration reveal a strong anisotropy for all samples with the LRD40 sample exhibiting the most distinct features. The relatively isotropic pattern observed in the *y*-beam configuration and the relatively large anisotropy observed in the *z*-beam configuration suggest that the clay platelets orient with their surface normal perpendicular to the film plane (*x*-*z* plane) for all compositions.

From 2D SANS patterns obtained in the two beam configurations, the intensity as a function of q can be calculated in the x, y, and z directions. The SANS intensity is averaged from 10° sectors in the horizontal (x) and vertical directions (y or z) of the 2D SANS pattern with the intensity averaged in the horizontal x direction overlapping perfectly. This procedure allows the SANS intensities in all three directions to be compared (Fig. 3). All SANS intensities were without incoherent scattering corrections. For all PEO-LRD films, a maximum at $q_{max} \approx 0.01$ Å^{-1} corresponding to a d-spacing, $d = 2\pi/q_{max}$, on the order of 600 Å was observed, and this was most pronounced in the y direction. It is difficult to determine the exact peak positions because of smearing from the form factor. The maximum is observed best in the y direction for LRD40 at $d = (644 \pm 15)$ Å. Intensities in the y direction are significantly stronger than those observed in the x direction. A visual inspection of data obtained in the z-beam configuration suggests that the composition strongly influences the degree of clay orientation and the film morphology.

It is of interest to compare the orientations in polymer–clay solutions determined in our previous study[36] with those in the films. This could offer insight into the origin and mechanisms for the orientation in nanocomposite films. The LRD fully exfoliates in PEO solution with the polymer keeping the clay platelets apart at a specific correlation length. From solution orientation mea-

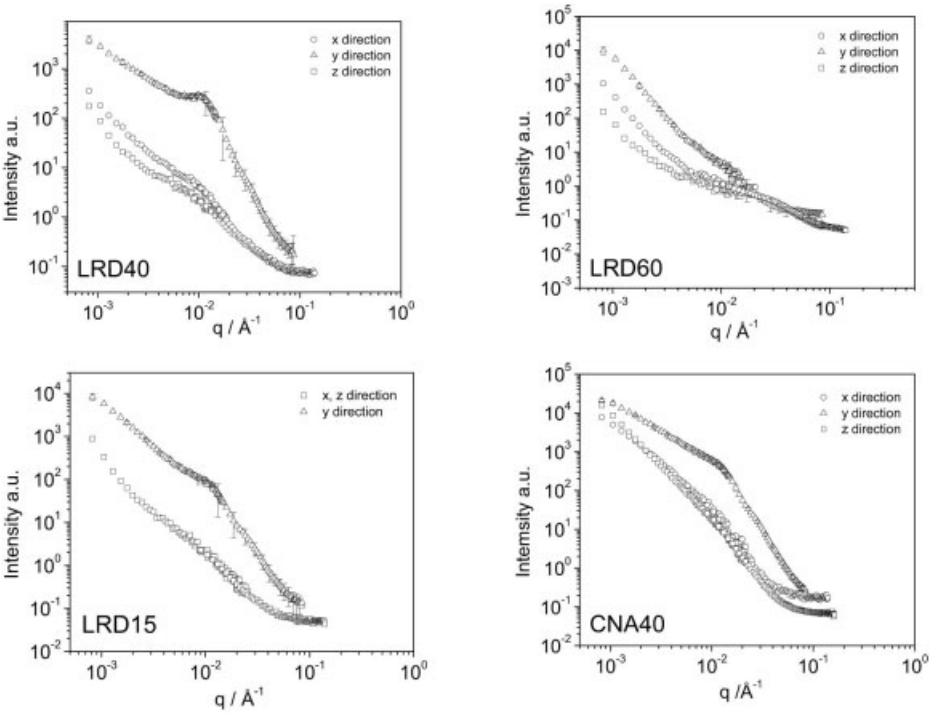

Figure 3. SANS intensity as averaged in 10° sectors for all three directions in space. Isotropic SANS data such as Figure 2(e,g) are circularly averaged. In this case, intensities in the z and x directions are the same. Intensities in the x direction or circularly averaged data cover a larger q range than intensities in the y or z direction. This is due to an off-centered beamstop (see Fig. 2). Data were placed on the same arbitrary scale.

surements under shear, we know that during the spreading process, the polymer chains stretch and restrict the mobility of the platelets. In addition, an unusual alignment of the clay platelets along the flow direction with the surface normal in the vorticity direction ('a' orientation) was observed.[36] The relaxation after cessation of shear is not well understood. Although SANS studies on PEO-LRD solutions observed very fast relaxation of anisotropy, stress-relaxation measurements showed that full relaxation occurs at very long times. Upon drying, the predominant clay orientation is the c direction. Those studies suggested that during the drying process, the network collapses and the concentration changes significantly, and relaxation as observed in solution is slowed down. Although manual spreading continues with incompletely dried films,[45] platelets orient and do not randomize as they would in solution.

Scattering patterns from films in the y-beam configuration demonstrate some anisotropy for LRD40 and LRD60 [Fig. 2(a,b)], suggesting that even with the collapse of the network, a small amount of solution-like orientation is preserved in the films. This may be attributed to strong concentration changes during the drying process, which reduce the rate of relaxation or randomization of the platelets. SANS patterns obtained in the y-beam configuration from LRD15 and CNA40 multilayer films were isotropic. The LRD15 and CNA40 samples showed the c orientation in both solution[52] and in films, whereas the LRD60 and LRD40 samples exhibited different orientation in solution (a orientation) and in films (c orientation) (see Table 2).

Figure 4 portrays the intensity versus q plot from the PEO-LRD films with various LRD con-

Table 2. Clay Orientation in Solution[36,37,52] and in Film

Sample	Orientation in Film	Orientation in Solution
LRD15	c	c
LRD40	c (a)	a
LRD60	c (a)	a
CNA40	c	c

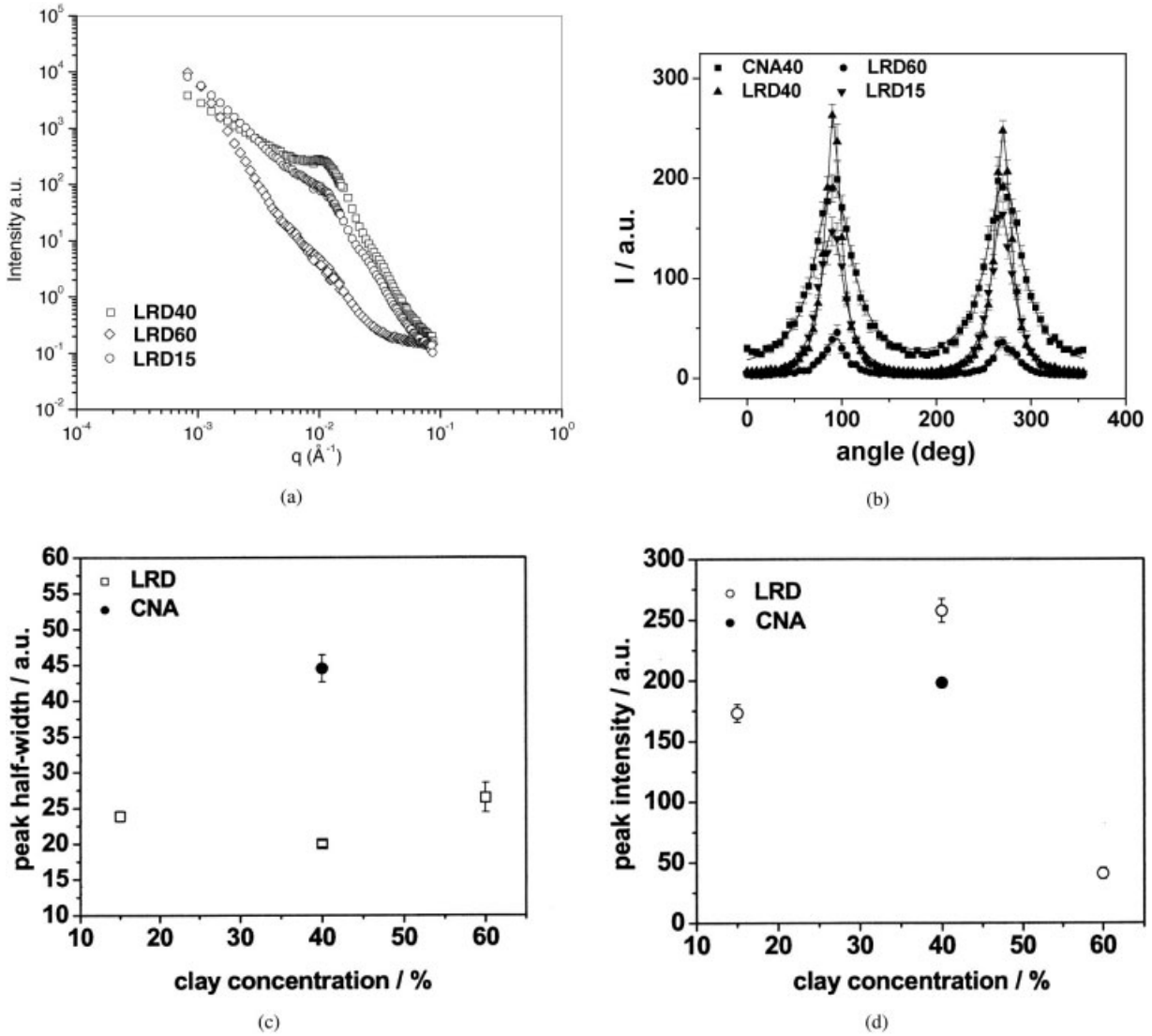

Figure 4. (a) LRD series: concentration dependence for $I(q)$ versus q as averaged in the y direction. An estimated relative error for maxima or shoulders is given in the text. Error bars for these intensities are shown in Figure 3. (b) Azimuthal scans of scattered intensity at $q = 0.0031$ Å^{-1} (SANS configuration: 15 m) and Lorentzian fit. (c) Half-width of azimuthal intensity as function of clay concentration.

tents averaged in the y direction. A maximum or shoulders occurs at (614 ± 50) Å for LRD15, (644 ± 15) Å for LRD40, and (630 ± 70) Å for LRD60, suggesting the spacing is relatively independent of the clay concentration. From solution studies, we know that excess polymer chains remain free in the solution and do contribute mechanically once the clay platelets are saturated with the polymers. The network in solution consists of clay-rich and clay-poor domains.[37,39] The critical concentration occurs at 3% LRD by mass fraction and 2% PEO by mass fraction in solution, corresponding to 60% LRD by mass fraction in the film. The shoulder or maximum observed in this SANS data on films corresponds to correlation in the lateral packing of domains consisting of clay sequestered in polymer. A larger polymer composition should result in higher d-spacing, but this was not observed in our system. The LRD40 sample appears to have the optimal polymer to clay ratio that leads to the most pronounced SANS anisotropy and stronger correlation than for

LRD15 and LRD60. Parameters that may contribute to higher SANS anisotropy for LRD40 are concentration of the clay combined with strong polymer–clay interactions, polymer molecular mass and chain flexibility of PEO, the type of deformation, and crystallization of the polymer. The relationship between clay orientation and orientation of other structural units such as polymer unit cells and polymer lamellae remains unclear but will be the subject of future investigation.

For comparison, CNA40 (d = 628 Å ± 70 Å) and LRD40 (d = 644 Å ± 15 Å) films that have similar polymer to clay ratios but differ in the clay type and aspect ratio were examined. At the same clay mass fraction, the LRD sample will contain more particles than the montmorillonite sample. The SANS measurement showed that the orientation is stronger for the LRD sample than for the montmorillonite sample. This is counterintuitive because we expected the larger particles to align more preferentially than the smaller ones at a similar concentration. Rheological experiments in solution suggested that the network structure formed by the PEO and LRD is stronger than the network formed by PEO and montmorillonite.[52] The strength of the polymer–clay network in solution may strongly influence the alignment of clay during the film-spreading process.

The anisotropy in scattering patterns has been characterized in terms of peak heights and widths of azimuthal intensity profiles in which the peak height was used to assess the changes in molecular orientation.[20] With the same approach, data such as those presented in Figure 4(b) were fit with a Lorentzian curve, and the width and peak height are plotted as a function of clay concentration. The half-width at half-maximum decreased with increasing LRD concentration indicating that the degree of order increased with clay concentration. The half-width of CNA40 is also included for comparison. The peak height versus clay concentration shows a surprising behavior for LRD40.

The Hermans' orientation function (f)[53,54] or nematic-order parameter was also used to assess the degree of orientation

$$f = \frac{3\langle\cos^2\phi\rangle - 1}{2}$$

and

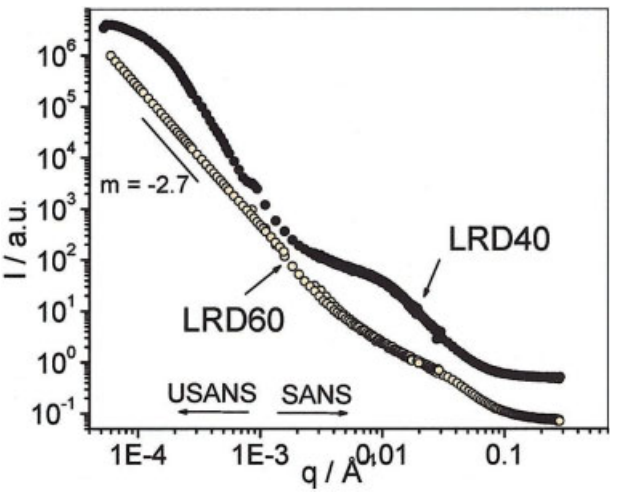

Figure 5. LRD40 and LRD60 reference bulk samples: circularly averaged $I(q)$ versus q from SANS and USANS data obtained over a large q range. An estimated relative error is about 4%.

$$\langle\cos^2\phi\rangle = \frac{\int_0^{\pi/2} I\cos^2\phi\,\sin\phi\,d\phi}{\int_0^{\pi/2} I\,\sin\phi\,d\phi} \qquad (1)$$

f was calculated with the azimuthally averaged data shown in Figure 4, where $\langle\cos^2\phi\rangle$ is the average cosine squared weighted by intensity I as a function of the radial angle, ϕ. A system is completely aligned when f = 1 and random when f = 0. For q = 0.0031 Å^{-1} (SANS configuration: 15 m), f = 0.41 for LRD15, f = 0.46 for LRD40, f = 0.38 for LRD60, and f = 0.51 for CNA40. On the basis of these calculations, the degree of alignment was significantly greater for LRD40 than for LRD15 and LRD60, which are comparable. In addition, the PEO-LRD film was considerably more aligned than the PEO-CNA film with the same clay mass fraction (Figure 2).

Figure 5 displays combined SANS and USANS[55] intensity profiles for bulk samples LRD40 and LRD60 over a large q range. LRD60 is characterized by $I(q) \propto q^{-2.7}$ in the low USANS q range and a shoulder at about 0.02 Å^{-1}, which corresponds to the spacing between polymer-covered clay plates. This structure can be observed by AFM. Because of the special experimental data collection of USANS, it is not easy to explain these data (desmeared USANS data were used here).[55] A qualitative interpretation of the data

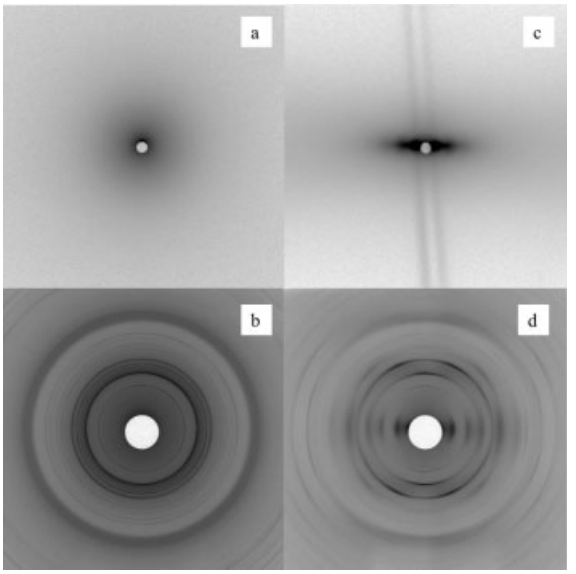

Figure 6. SAXS and WAXS for LRD40 measured parallel and perpendicular to the spread direction: (a) SAXS perpendicular to the spread direction, (b) WAXS perpendicular to the spread direction, (c) SAXS parallel to the spread direction, and (d) WAXS parallel to the spread direction. The stripe in c is an experimental artifact.

allows some speculations. The collapse of a 3D network from solution leads to fractal structures in three dimensions. In an oriented film, however, fractal structures are observed in two dimensions (x-z plane) as observed with SEM.[47] Fractal structures influence the total scattering intensity and the scaling behavior. Scattering data on LRD40 showed onsets for at least two maxima. The maximum at high q can be correlated with the spacing between clay platelets. The maximum at very low q originates from individual large micro-meter-sized clusters. The shapes of SANS intensities versus q from manually oriented micrometer thick films (x,z plane, anisotropic pattern) and millimeter thick bulk samples (x,z plane, isotropic pattern) were significantly different (Figs. 2, 3, and 5). This demonstrates that manual spreading influences the orientation of clay platelets strongly.

Preliminary SANS annealing studies on LRD40 and LRD60 (not shown here) indicated that SANS intensities did not change with increasing temperature up to 100 °C. At very high temperatures (>200 °C), polymer degradation was observed and once-transparent samples turned slightly yellow.

SAXS and WAXD were also used to examine the orientation in PEO-LRD nanocomposite films. Figure 6 shows 2D SAXS and WAXD profiles for a LRD40 film measured perpendicular and parallel to the spread direction. Both SAXS and WAXD profiles measured perpendicular to the spread direction were isotropic, whereas those measured parallel to the spread direction were highly anisotropic. Although a small degree of anisotropy was detected by the SANS measurement, which probed a much lower q range, SAXS did not detect anisotropy in the z direction.

Perhaps the more interesting profiles are those obtained with WAXD in which the PEO crystal structures as well as interplatelet spacings can be assessed. The typical crystalline structure of pure PEO is a well-known monoclinic lattice with WAXD showing several orders of diffraction [many observed diffraction peaks are numbered in Figures 7 and 8(a)]. The relative intensity versus 2θ obtained in WAXD for LRD40 were calculated in the x, y, and z directions (Figs. 7 and 8). Interestingly, the diffraction profiles obtained in the x and z directions exhibited signatures for PEO crystallites but lacked peaks 4 and 5 as would be expected in pure PEO. The scattering profile obtained in the y direction was significantly different from those profiles obtained in the x and z directions, indicating that this sample is highly oriented. The peaks observed in the y direction corresponded to distances between the clay platelets. These results suggested that the clay platelets are oriented with their surface normal to the film spread direction, and this agreed

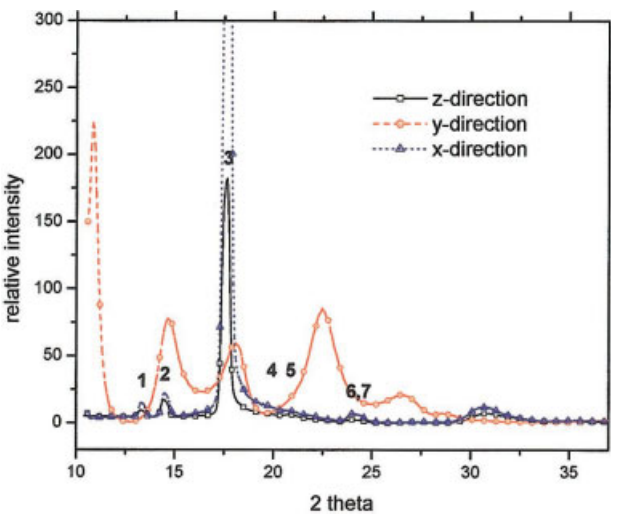

Figure 7. WAXD pattern of LRD40 measured in the x, y, and z directions. [Color figure can be viewed in the online issue, which is available at www.interscience.wiley.com]

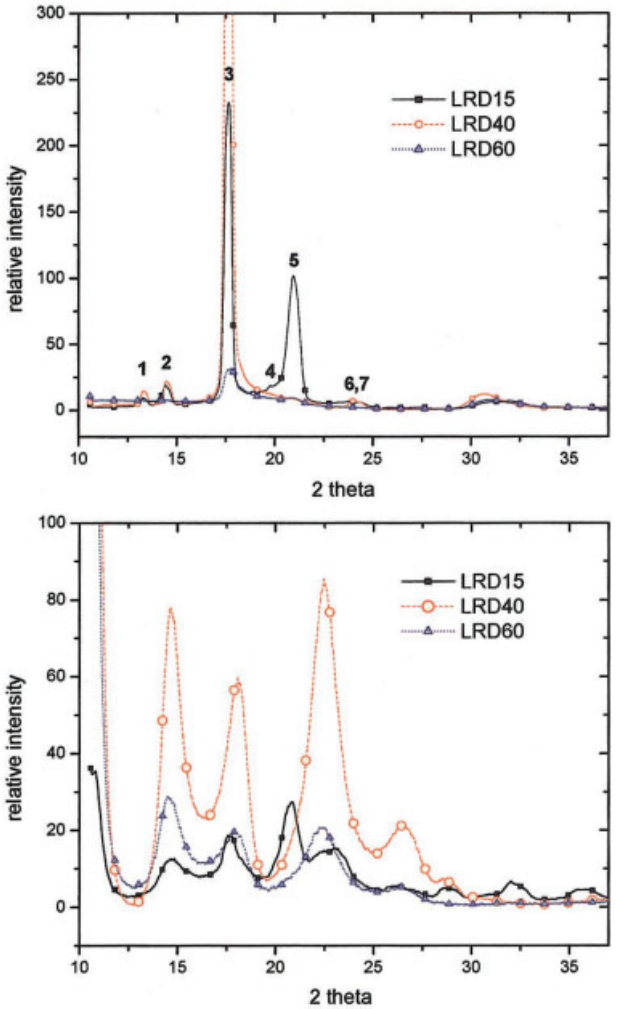

Figure 8. WAXD pattern of PEO-LRD nanocomposites with various clay contents measured in the (a) *x* direction and (b) *y* direction. [Color figure can be viewed in the online issue, which is available at www.interscience.wiley.com]

with our SANS results. In addition, the results obtained in the *x* direction suggested the crystalline PEO is also oriented and is orthogonal to the orientation of the clay platelet.

The WAXDs of PEO-LRD nanocomposites with 15, 40, and 60% LRD by mass fraction measured in the *x* and *y* directions are shown in Figure 8(a,b), respectively. Comparisons of diffraction patterns showed mostly PEO crystalline structures in the *x* direction, but the diffraction pattern was more complex in the *y* direction. In the *x* direction [Fig. 8(a)], PEO-LRD with the lowest LRD mass fraction (15%) showed a number of distinct PEO diffraction peaks. Surprisingly, LRD40 did not show peaks 4 and 5, but the relative intensity for peak 3 was significantly stronger than that measured for LRD15. The disappearance of peaks 4 and 5 may be attributed to the high orientation of PEO crystal structures. At even higher clay composition, LRD60, the sample becomes mostly amorphous as all crystalline peaks essentially disappear. The diffraction profiles in the *y* direction exhibit a number of peaks not associated with PEO crystal structures, but with interparticle spacing for all clay compositions. This suggests that the clay platelets are oriented at all compositions. The relative intensity was highest for LRD40 indicating that this composition exhibits the strongest orientation, in agreement with the SANS data.

The orientation of the clay particles and possibly the presence of voids that were generated during the drying process may influence the total scattering intensity as well as the position of intensity peaks. The onset for a second maximum cannot be explained at this moment (Figure 4a). This will be investigated in the future.

LRD40 and LRD60 are hygroscopic transparent and strongly birefringent films that have to be stored in a dry environment. Crystallinity of representative films, determined by DSC, changed within 0.5 year from about 0 to 2.8% for LRD60 and from 40.1 to 40.4% for LRD40, showing that the sample structure did not change significantly over time. Extensive crystallinity and birefringence studies are not the scope of this article but will be discussed in the future.[47]

CONCLUSIONS

The orientation of platelets in micro-meter-thick PEO-clay nanocomposite films with various clay contents was investigated with scattering and diffraction measurements. Polymer–clay solutions were used to prepare nanocomposite films with defined clay orientations and high clay contents (60% by mass fraction), which are difficult to prepare by other methods. The mechanism for the observed clay orientation is as follows. During the drying process, the polymer–clay network collapses and clay platelets are shear-oriented, preferentially in the spread direction. Some solution LRD orientation is maintained in the film during the drying process at high clay concentration. Surprisingly, large montmorillonite particles aligned less than the smaller LRD particles at a similar concentration. We concluded that the strength of the polymer–clay network strongly

influences the alignment of clay during the film-spreading process. As the solvent leaves, clay-clay interactions, which should be very strong above 5–10%, will play a dominant role in determining the orientation in response to shear, with these likely favoring the orientation of platelets with their surface normal perpendicular to the plane of the film.

We have shown that the presence of oriented and dispersed nano-meter-sized clay particles in a PEO film strongly affects the structure, but material properties such as mechanical, optical, and permeability are also influenced. Some of the films discussed above were transparent and showed strong birefringence, which made them suitable for optical components. These properties will be presented in a future article.[47] Because the clay as well as the polymer component are hygroscopic, the reversible absorption of water by a multilayered polymer–clay film makes the material interesting as a humidity sensor.[40] Although PEO was the only polymer study here, some of the nanocomposite films do not significantly degrade at temperatures up to 200 °C, suggesting they have good thermal properties. Preliminary results have suggested that at very high clay concentrations, rheological experiments with conventional rheometers are not possible because of excessively high moduli and sample toughness. Films containing 60% of silicate by mass and higher may be used as precursors for future ceramic materials, microelectronics, and anisotropic electric insulators. These are all issues that will be addressed in future research.

The authors acknowledge the support of NIST and the National Science Foundation (NSF), through agreement DMR 9986442, in providing the neutron research facilities used in this work. Research carried out at the NSLS, BNL, was supported by the U.S. Department of Energy, Division of Materials Sciences and Division of Chemical Sciences, under contract DE-AC02-98CH10886. The authors thank John Barker for doing preliminary USANS experiments; Igors Sics and Shaofeng Ran for facilitating the 1D and 2D SAXS–WAXD measurements on beamlines X27C and X3(2A), respectively; and Forrest A. Landis for his helpful discussions. The authors also acknowledge financial support from the Louisiana Board of Regents: LEQSF (2002-05)-RD-A-09 and by our IGERT program. Oak Ridge National Laboratory is managed by the U.S. Department of Energy by UT-Batelle LLC under contract DE-AC0500OR22725. Finally, the authors thank the reviewers for their helpful comments.

REFERENCES AND NOTES

1. Krishnamoorti, R.; Vaia, R. A. Polymer Nanocomposites; American Chemical Society: Washington, DC, 2002; Vol. 804.
2. Gabriel, J. C. P.; Davidson, P. Adv Mater 2000, 12, 9.
3. Schmidt, G.; Malwitz, M. M. Curr Opin Colloid Interface Sci 2003, 8, 103–108.
4. Krishnamoorti, R.; Yurekli, K. Curr Opin Colloid Interface Sci 2001, 6, 464–470.
5. Kojima, Y.; Usuki, A.; Kawasumi, M.; Okada, A.; Fukushima, Y.; Kurauchi, T.; Kamigaito, O. J Mater Res 1993, 8, 1185–1189.
6. Chapman, R.; Mulvaney, P. Chem Phys Lett 2001, 349, 358–362.
7. Wilson, O.; Wilson, G. J.; Mulvaney, P. Adv Mater 2002, 14, 1000.
8. Yoon, P. J.; Fornes, T. D.; Paul, D. R. Polymer 2002, 43, 6727–6741.
9. Giannelis, E. P.; Krishnamoorti, R.; Manias, E. Adv Polym Sci 1999, 138, 107–147.
10. Burnside, S. D.; Giannelis, E. P. Chem Mater 1995, 7, 1597–1600.
11. Burnside, S. D.; Giannelis, E. P. J Polym Sci Part B: Polym Phys 2000, 38, 1595–1604.
12. Lee, D. C.; Jang, L. W. J Appl Polym Sci 1998, 68, 1997–2005.
13. Gilman, J. W. Appl Clay Sci 1999, 15, 31–49.
14. Pinnavaia, T.; Beall, G. Polymer–clay Nanocomposites; Wiley: New York, 2001.
15. Lagaly, G. Appl Clay Sci 1999, 15, 1–9.
16. Luckham, P. F.; Rossi, S. Adv Colloid Interface Sci 1999, 82, 43–92.
17. Burnside, S. D.; Wang, H. C.; Giannelis, E. P. Chem Mater 1999, 11, 1055–1060.
18. Gabriel, J. C. P.; Camerel, F.; Lemaire, B. J.; Desvaux, H.; Davidson, P.; Batail, P. Nature 2001, 413, 504–508.
19. Hongladarom, K.; Ugaz, V. M.; Cinader, D. K.; Burghardt, W. R.; Quintana, J. P.; Hsiao, B. S.; Dadmun, M. D.; Hamilton, W. A.; Butler, P. D. Macromolecules 1996, 29, 5346–5355.
20. Dadmun, M. D.; Han, C. C. Macromolecules 1994, 27, 7522–7532.
21. Schmidt, G.; Muller, S.; Schmidt, C.; Richtering, W. Rheol Acta 1999, 38, 486–494.
22. Walker, L. M.; Wagner, N. J. Macromolecules 1996, 29, 2298–2301.
23. Butler, P. Curr Opin Colloid Interface Sci 1999, 4, 214–221.
24. Bates, F. S.; Koppi, K. A.; Tirrell, M.; Almdal, K.; Mortensen, K. Macromolecules 1994, 27, 5934–5936.
25. Schmidt, G.; Richtering, W.; Lindner, P.; Alexandridis, P. Macromolecules 1998, 31, 2293–2298.
26. Percy, M. J.; Amalvy, J. I.; Barthet, C.; Armes, S. P.; Greaves, S. J.; Watts, J. F.; Wiese, H. J Mater Chem 2002, 12, 697–702.

27. Amalvy, J. I.; Percy, M. J.; Armes, S. P.; Wiese, H. Langmuir 2001, 17, 4770–4778.
28. Fong, H.; Liu, W. D.; Wang, C. S.; Vaia, R. A. Polymer 2002, 43, 775–780.
29. Jimenez, G.; Ogata, N.; Kawai, H.; Ogihara, T. J Appl Polym Sci 1997, 64, 2211–2220.
30. Ogata, N.; Jimenez, G.; Kawai, H.; Ogihara, T. J Polym Sci Part B: Polym Phys 1997, 35, 389–396.
31. Kojima, Y.; Usuki, A.; Kawasumi, M.; Okada, A.; Kurauchi, T.; Kamigaito, O.; Kaji, K. J Polym Sci Part B: Polym Phys 1994, 32, 625–630.
32. Bafna, A.; Beaucage, G.; Mirabella, F.; Mehta, S. Polymer 2003, 44, 1103–1115.
33. Varlot, K.; Reynaud, E.; Kloppfer, M. H.; Vigier, G.; Varlet, J. J Polym Sci Part B: Polym Phys 2001, 39, 1360–1370.
34. Lele, A.; Mackley, M.; Galgali, G.; Ramesh, C. J Rheol 2002, 46, 1091–1110.
35. Okamoto, M.; Nam, P. H.; Maiti, P.; Kotaka, T.; Hasegawa, N.; Usuki, A. Nano Lett 2001, 1, 295–298.
36. Schmidt, G.; Nakatani, A. I.; Butler, P. D.; Han, C. C. Macromolecules 2002, 35, 4725–4732.
37. Schmidt, G.; Nakatani, A. I.; Butler, P. D.; Karim, A.; Han, C. C. Macromolecules 2000, 33, 7219–7222.
38. Schmidt, G.; Nakatani, A. I.; Han, C. C. Rheol Acta 2002, 41, 45–54.
39. Lin-Gibson, S.; Schmidt, G.; Kim, H.; Han, C. C.; Hobbie, E. K. Manuscript submitted, 2003.
40. Kleinfeld, E. R.; Ferguson, G. S. Chem Mater 1995, 7, 2327–2331.
41. http://www.scprod.com/.
42. http://www.nanoclay.com/.
43. Ramsay, J. D. F.; Swanton, S. W.; Bunce, J. J Chem Soc Faraday Trans 1990, 86, 3919–3926.
44. Pignon, F.; Magnin, A.; Piau, J. M.; Cabane, B.; Lindner, P.; Diat, O. Phys Rev E: Stat Phys Plasmas Fluids Relat Interdiscip Top 1997, 56, 3281–3289.
45. Single films with an average layer thickness of a few micrometers were obtained by manually spreading the filled polymer gel on a glass substrate with a blade. Every few hours, one film was spread and dried, which gave about 7–10 layers a day. During the drying process, the films were manually oriented by respreading the already half-dried films. Samples were dried in desiccators overnight. Films with the same spread direction were dried layer by layer onto each other until a total multilayer film of about 1 mm was obtained. Then, the total thickness was measured with a caliper and divided by the number of layers. This procedure was done for several samples giving thicknesses of 5–7 μm for each single film. The film uncertainty was about 20% and was calculated as an average from several samples. A mechanical spreader could not be used because of high viscosity and gumlike sample behavior.
46. Glinka, C. J.; Barker, J. G.; Hammouda, B.; Krueger, S.; Moyer, J. J.; Orts, W. J. J Appl Crystallogr 1998, 31, 430–445.
47. Malwitz, M. M.; Butler, P. D.; Henk, M. C.; Schmidt, G. Manuscript submitted for publication, 2003.
48. van Duffel, B.; Schoonheydt, R. A.; Grim, C. P. M.; De Schryver, F. C. Langmuir 1999, 15, 7520–7529.
49. Decher, G. Science 1997, 277, 1232–1237.
50. Decher, G.; Schlendorff, J. Multilayer Thin Films: Sequential Assembly of Nanocomposite Materials; VCH: Verlagsgesellschaft, Germany, 2003.
51. Kleinfeld, E. R.; Ferguson, G. S. Science 1994, 265, 370–373.
52. Malwitz, M. M.; Butler, P. D.; Schmidt, G. Manuscript submitted for publication, 2003.
53. Hermans, P. H.; Hermans, J. J.; Vermaas, D.; Weidinger, A. J. J Polym Sci 1947, 3, 393–406.
54. Hermans, P. H.; Kolloid-Zeitschrift 1941, 97, 223–228; and de Booys, J.; Hermans, P. H. Kolloid-Zeitschrift 1941, 97, 229–231.
55. USANS is only a minor part of this article; therefore, the experimental setup and data collection are not explicitly defined. Here, we demonstrate only preliminary results. Much more will be presented in a future publication.